Analysis of Upper-Tropospheric Water Vapor Brightness Temperatures from SSM/T2, HIRS, and GMS-5 VISSR

WESLEY BERG

Cooperative Institute for Research in Environmental Sciences, University of Colorado, Boulder, Colorado

JOHN J. BATES

NOAA, Climate Diagnostics Center, Boulder, Colorado

DARREN L. JACKSON

Cooperative Institute for Research in Environmental Sciences, University of Colorado, Boulder, Colorado

(Manuscript received 27 October 1997, in final form 30 July 1998)

ABSTRACT

Satellite microwave and infrared instruments sensitive to upper-tropospheric water vapor (UTWV) are compared using both simulated and observed cloud-cleared brightness temperatures (Tb's). To filter out cloudy scenes, a cloud detection algorithm is developed for the Special Sensor Microwave/Temperature-2 (SSM/T2 or T2) data using the 92- and 150-GHz window channels. An analysis of the effect of clouds on the T2 183-GHz channels shows sensitivity primarily to high clouds containing ice, resulting in significantly better sampling of UTWV Tb's over the convective zones and regions of persistent cloudiness. This is in contrast to the infrared sensors, which are extremely sensitive to any cloud contamination in the satellite field of view. A comparison of simulated UTWV Tb's from T2, the High-resolution Infrared Sounder (HIRS), and the Visible Infrared Spin Scan Radiometer (VISSR) indicates a higher overall sensitivity to changes in UTWV in the T2 channel. HIRS and VISSR, however, are more sensitive to moisture at higher levels. Cloud-cleared Tb's from T2 and HIRS were found to be highly correlated in the tropical dry zones and in regions of strong seasonal variability but less correlated at higher latitudes. The advantages of the microwave T2 sensor for monitoring UTWV are demonstrated by its greater sensitivity to changes in upper-tropospheric moisture and superior coverage over cloudy regions.

1. Introduction

Upper-tropospheric water vapor (UTWV) is important for studies of weather and climate on a variety of time- and space scales. Synoptic meteorologists have used infrared UTWV imagery from geostationary satellites in a qualitative manner for many years. Tracking of UTWV features has long been used to derive water vapor drift winds for input to numerical weather prediction (NWP) schemes. These data have been useful in providing improved initialization to NWP (McNally and Vesperini 1996), and particularly, for improving hurricane track forecasting (Velden et al. 1997). More recently, these data have been used in direct one- and three-dimensional NWP assimilation schemes and have shown dramatic positive impact (A. P. McNally 1997, personal communication).

Infrared UTWV data have also been used in a variety of climate studies. Recent interest was sparked by Lindzen (1990), who challenged the notion that UTWV would provide a strong positive feedback to increases in temperature initiated by increases in anthropogenic greenhouse gases. This stimulated a reexamination of the satellite record of infrared UTWV observations. The High-resolution Infrared Sounder (HIRS) instruments on the National Oceanographic and Atmospheric Administration (NOAA) Polar-Orbiting Environmental Satellites (POES) have observed UTWV globally since 1979 using the upwelling radiance from the strong water vapor absorption line near 6.7 μm. Initially these data were not used because of large uncertainties in the atmospheric spectroscopy, specifically with regard to water vapor continuum effects, and because of disparities between these observations and in situ radiosonde observations. Recently, there has been considerable improvement in the atmospheric spectroscopy (Clough et

Corresponding author address: Dr. Wesley Berg, Cooperative Institute for Research in Environmental Sciences, University of Colorado, Campus Box 216, Boulder, CO 80309-0216.
E-mail: wkb@cdc.noaa.gov

al. 1992) and in our understanding of radiosonde observations of UTWV. This has led to increased use of both polar-orbiting and geostationary satellite observations of UTWV, although infrared observations are limited to clear or cloud-cleared fields of view since clouds are opaque in the infrared. This leads to a systematic bias in sampling UTWV, although Soden and Lanzante (1996) suggest that this bias is rather small.

At microwave frequencies, upwelling atmospheric radiation penetrates through nonprecipitating clouds with relatively low water content, such as cirrus. Theoretical studies (Rosenkranz et al. 1982; Wilheit 1990) and aircraft measurements (Wang et al. 1997) demonstrate that the water vapor resonance line at 183 GHz can be used to produce vertical profiles of water vapor by using measurements of several frequencies around the center of the line combined with information about the vertical temperature profile. Such an instrument, called the Special Sensor Microwave/Temperature-2 (SSM/T2 or T2), has now flown on the Defense Meteorological Satellite Program (DMSP) series of satellites for several years. A similar instrument will also fly on NOAA POES as part of the Advanced Microwave Sounding Unit (AMSU). Thus, there is a new opportunity for obtaining upper-tropospheric moisture, even in the presence of nonprecipitating clouds, and to compare these measurements to those from infrared water vapor sounders to help quantify the extent of the cloud bias problem.

A variety of differing philosophies have been used to extract climate information from long-term satellite observational datasets. There are a number of considerations to be made when choosing what type of analysis to perform on satellite sounder observations for climate applications. Perhaps two of the more important considerations are 1) the practical logistics of processing large amounts of satellite observations over an extended time period, and 2) the very important question of the influence of the first guess upon the retrieval, particularly the systematic errors. It is well known that for satellite-sounding instruments that have a strong overlapping of weighting functions, such as the instruments considered here, the direct solution to the inverse radiative transfer equation is unstable. To condition the inverse matrix so that the inversion is stable, a first guess to the solution is required. The first guess, however, results in a complex and systematic error structure related to the first guess (Eyre 1990).

As an alternative, many climate researchers have adopted a philosophy of examining the brightness temperature record from long-term satellite observations (Spencer and Christy 1993; Soden and Bretherton 1994; Bates et al. 1996). This method has the advantage of keeping the systematic error to a minimum as well as making the data-processing logistics much simpler. The main disadvantage of this approach is that all radiance information available is not used. In this paper we take the approach of examining satellite radiance information content for climate applications by comparing and contrasting radiative transfer simulations and observations of Tb's sensitive to UTWV from infrared and microwave observations. First, we describe the observational datasets. We then quantify the effects of clouds upon these data and present a method to detect and remove cloud effects from the microwave data. Next, we perform radiative transfer model simulation and sensitivity studies and compare these results with observations. Finally, we compare cloud-cleared upper-tropospheric Tb's for 1995 between the infrared HIRS channel 12 and the microwave T2 channel 2.

2. Dataset descriptions

UTWV data from a number of satellite sensors were used in this study. Infrared observations from HIRS channel 12 (6.7 μm) on NOAA POES and Visible Infrared Spin Scan Radiometer (VISSR) channel 4 (6.7 μm) on the Japanese Geostationary Meteorological Satellite (*GMS-5*) were compared with passive microwave data from T2 channel 2 (183 ± 1 GHz) on the DMSP satellites. The HIRS instrument has flown on nine satellites and has a nearly continuous data record from 1979 to the present, while the T2 has flown on three satellites starting in 1993. Although data from the geostationary satellites has been available for some time, because of difficulty in obtaining archived data from these sensors, only a short time period was available for this study. Cloud information derived from the *GMS-5* visible channel and the DMSP Special Sensor Microwave/Imager (SSM/I) was used in the development and validation of a cloud detection technique for the T2 data.

a. Radiosonde profiles

A set of 1761 radiosonde profiles called the TIROS initial guess atmospheres (TIGR-2) was used to compute many of the simulated results. The TIGR-2 profiles were formulated using a Dynamic Clusters Method (Moine et al. 1987). This method clustered the radiosonde data by airmass type into five separate airmass classes: tropical, midlatitude, cold midlatitude, polar, and winter-polar atmospheres. The advantage of this method is that it finds ''strong patterns'' within each class so as to provide a wide array of atmospheric conditions for any given class, not just the mean. These data are therefore very useful for doing forward radiative transfer simulations. In addition, high vertical resolution soundings from a NOAA Combined Sensor Program (CSP) Environmental Technology Laboratory (ETL) cruise over the western and central Pacific (15 March–12 April 1996) and a Pan-American Climate Studies (PACS) cruise over the eastern Pacific (7 July–27 August 1997) were used in this study.

b. DMSP SSM/T2

The SSM/T2 or T2 instrument is an operational passive microwave water vapor sounder on board the

DMSP *F11, F12,* and *F14* satellites. The DMSP satellites are in sun-synchronous near-polar orbits, providing nearly global daily coverage. The T2 consists of a total of five channels: three centered around the 183.31-GHz water vapor line at 183.31 ± 1, 183.31 ± 3, and 183.31 ± 7 GHz and two window channels at 91.665 and 150.0 GHz. This study uses UTWV data from channel 2 (183 ± 1 GHz), which is primarily sensitive to moisture above 500 mb. The 92- and 150-GHz window channels are used in the development of a cloud detection algorithm. The instrument is a cross-track scanner taking 28 observations across each scan with an approximate resolution of 48 km and a total swath width of 1400 km. A continuous archive of T2 data is available starting with *F11* in April 1993. The T2 sensor is currently operating on board the DMSP *F12* and *F14* satellites. Unfortunately, a problem with the 92-GHz channel on board *F11* means that a cloud detection technique developed using the 92- and 150-GHz channels cannot be applied prior to the availability of *F12* data starting in October 1994.

c. NOAA HIRS

The HIRS instrument has resided on NOAA series polar-orbiting satellites since November 1978. Its primary function is the measurement of infrared radiation at bands used to retrieve vertical profiles of temperature and water vapor. The HIRS instrument is a cross-track scanner with 56 observations across each scan and a pixel resolution of approximately 30 km at nadir, resulting in a total swath width of 2250 km. The substantially wider swath coverage of the HIRS instrument over the T2 results in greater coverage from a single satellite. This study considers only HIRS channel 12, which is centered near the 6.7-μm water vapor line and is most sensitive to changes in upper-tropospheric (200–500 mb) water vapor. The data originated from the National Environmental Satellite Data and Information Service (NESDIS) operational sounding product as cloud-cleared radiances. HIRS data from 1995 used in the comparison with T2 included cloud-cleared radiances from *NOAA-11, -12,* and *-14.* Further details on these data can be found in Kidwell (1995). Data from the operational product dataset were subjected to various quality controls including cloud clearing and satellite intercalibration, which are described at length by Bates et al. (1996).

d. GMS-5 VISSR

High spatial and temporal resolution observations of UTWV Tb's are currently available from a number of geostationary weather satellites including several of the U.S. Geostationary Operational Environmental Satellites (GOES) and European Meteosats, as well as the latest Japanese *GMS-5* and the new Chinese *FY-2.* Due to difficulty in obtaining long time series from these various sources, only data from the 6.7-μm infrared channel on the Japanese *GMS-5* VISSR is used in this study. The comparison with *GMS-5,* however, was confined to simulated Tb's and qualitative observations as a result of limited data availability and no cloud-clearing technique. The high spatial (8 km) and temporal (3-h full disk) sampling, however, is valuable for providing information on diurnal variability.

3. Cloud detection and clearing

Due to differences in the sensitivity of the infrared HIRS instrument and the microwave T2 to clouds, it is necessary to detect and remove cloud-contaminated pixels so that a meaningful comparison can be made. The HIRS sounding product data utilized the cloud-clearing method of McMillin and Nappi (1986). For the T2, a cloud detection algorithm was developed and subsequently applied to the data.

a. HIRS cloud-clearing algorithm

The NESDIS cloud-clearing algorithm utilizes the method described in McMillin and Dean (1982) and modified in McMillin and Nappi (1986). This method determines clear-sky soundings by performing empirical cloud tests on a 7 × 9 block of HIRS pixels. If one or more pixels within the block are determined to be clear sky, the radiances of all the clear-sky pixels are averaged together to determine the clear-sky radiance. After March 1992, NESDIS also produced a high-resolution sounding dataset by performing these tests on a 3 × 3 block of pixels. These high-resolution soundings were used for the comparisons done in this paper. If none of the pixels within the selected block are deemed to be clear sky, the *N* Star (*N**) method is attempted. This method calculates a clear-sky radiance in cloudy regions by assuming that cloud and surface properties remain constant and only the cloud fraction changes between adjacent pixels. If the *N** method is successful, then all *N** clear-sky radiances and clear-sky radiances are averaged to determine a clear-sky radiance. Even though this battery of tests does fairly well in detecting clouds, some cloud types are difficult to detect. For example, low clouds at night are hard to sense in the IR, thin cirrus clouds at any time are hard to detect, and very cold regions can be mistakenly flagged as cloudy.

Unfortunately, observations contaminated by precipitation in the HIRS operational sounding dataset were discarded. As a result, information on the total number of soundings over regions with precipitation, such as the western Pacific warm pool, was not available. To produce estimates of the total number of HIRS soundings, and thus the percentage of clear-sky observations, raw level-1b HIRS data was used. Estimates of the total number of soundings were determined by computing the total number of pixels from the level-1b data within each 2.5° × 2.5° bin for each of the 73 pentads (5-day

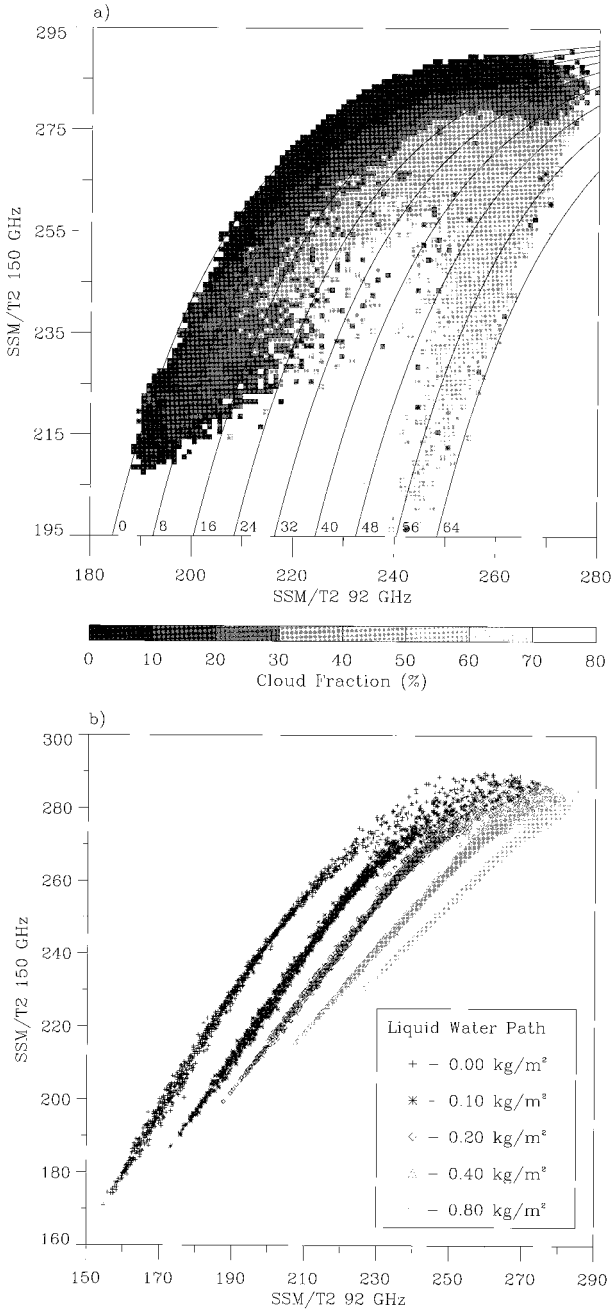

FIG. 1. Variations in cloud amount as a function of both the 92- and 150-GHz T2 window channels determined from different sources. (a) Observed Tb's and the associated cloud fraction within a T2 pixel derived from *GMS-5* visible data. (b) Simulated Tb's computed from the TIGR-2 profiles using a radiative transfer model with the cloud liquid water path prescribed within a very simple cloud parameterization. Lines of constant T2 cloud index values are also shown in (a).

periods) during 1995. For each block of 40 scans (with 56 pixels per scan), a total of 180 soundings are produced. Using the ratio 180/(40 × 56), therefore, estimates of the total number of soundings were computed from the level-1b pixel count data.

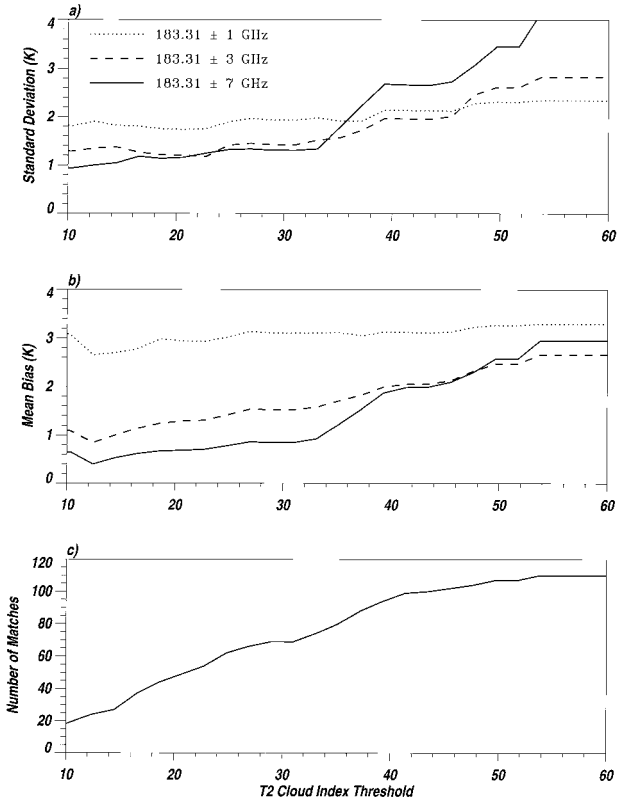

FIG. 2. (a) Mean difference, (b) standard deviation, and (c) number of observations computed from a comparison of simulated and observed Tb's for the three T2 183-GHz channels. The simulated radiance values were computed from radiosonde measurements taken during two different field campaigns over the Pacific. The statistics are computed based on the total number of observed values below the threshold value specified along the abscissa.

b. Development of a cloud detection algorithm for SSM/T2

Although microwave Tb's observed by T2 are significantly less sensitive to thin cirrus and other nonprecipitating clouds than HIRS, clouds with significant liquid water or ice complicate the water vapor signal, thus requiring nonlinear retrieval techniques (Wilheit 1990). Therefore, observations contaminated by clouds must first be removed in order to investigate variability in UTWV and/or compare with IR water vapor measurements. A technique for identifying and removing cloud contaminated pixels from the T2 data was developed using a combination of visible data from the Japanese *GMS-5* geostationary weather satellite and simulated Tb's from the TIGR-2 profiles.

1) DETERMINATION OF CLOUD FRACTION FROM GMS-5

High-resolution (8 km) *GMS-5* visible data for the period from 16 March–12 April 1996 were used to compute cloud fraction corresponding to the T2 pixels. The

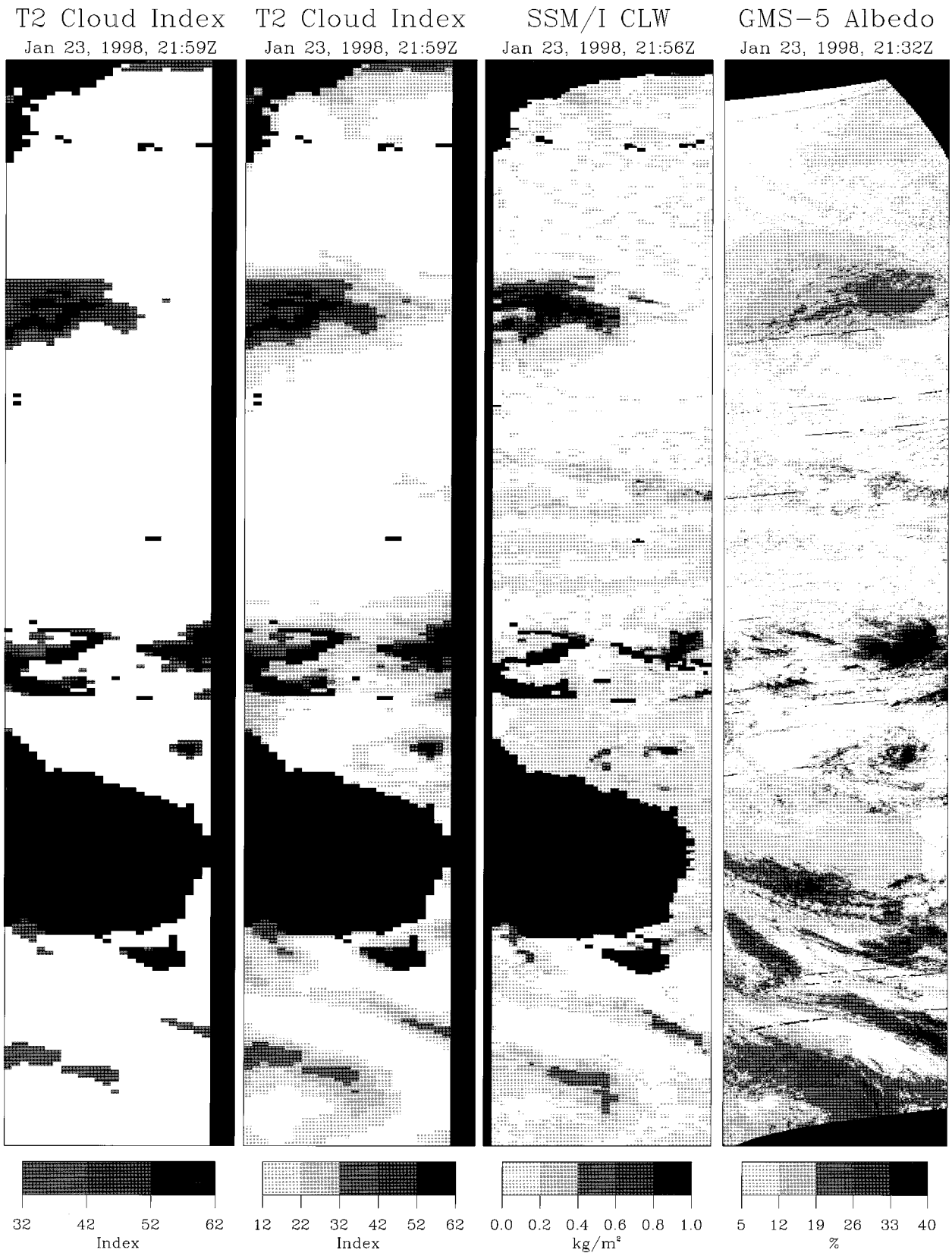
T2 Cloud Index
Jan 23, 1998, 21:59Z
T2 Cloud Index
Jan 23, 1998, 21:59Z
SSM/I CLW
Jan 23, 1998, 21:56Z
GMS-5 Albedo
Jan 23, 1998, 21:32Z
32 42 52 62
Index
12 22 32 42 52 62
Index
0.0 0.2 0.4 0.6 0.8 1.0
kg/m²
5 12 19 26 33 40
%

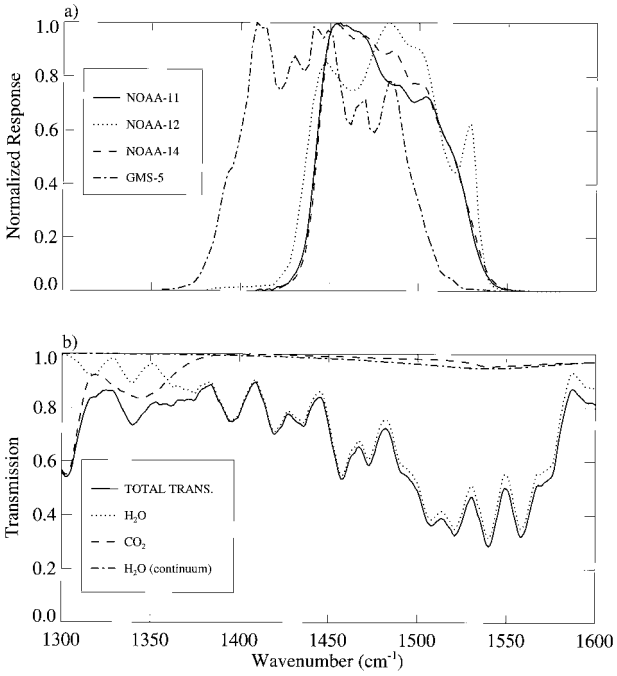

FIG. 4. (a) Normalized spectral response functions for HIRS channel 12 on *NOAA-11, -12,* and *-14* and VISSR channel 4 on *GMS-5*. (b) Modeled total atmospheric transmission from 300 mb to top of atmosphere for a standard tropical atmosphere. Also shown is the transmission for individual gases such as water vapor (H_2O), water vapor continuum (H_2O CON), and carbon dioxide (CO_2).

visible channel data was corrected for the sun angle using an empirical correction based on the cosine of the solar zenith angle and matched to the individual T2 pixels. Due to variations in the T2 pixel size from nadir to the limb, the number of *GMS-5* pixels corresponding to each T2 pixel varied between 15 and 50. Visible radiance values with a solar zenith angle greater than 60° were not used in the comparison. The region of the collocated *GMS-5* and T2 data extended from 30°S to 50°N and 75°E to 165°W over ocean only since surface emission effects can produce ambiguity in the cloud signal over land surfaces. A cutoff time of 30 min was used for the collocated T2 and *GMS-5* pixels, resulting in a total of 69 T2 overpasses during the month. Of these collocated scans, several were discarded due to the presence of sun glint in the *GMS-5* visible data leaving a total of 53 collocated scans used in the comparison.

A visible albedo threshold of 5% was used to determine clear/cloudy pixels. The 5% threshold value was chosen with respect to the minimum observed value within a corresponding 5° × 5° box in order to account for slight regional variations in the clear-sky background albedo. The 5% threshold was arrived at by a qualitative analysis and comparison with cloud liquid water (CLW) retrievals from SSM/I (Weng and Grody 1994). Cloud fraction for each T2 pixel was then computed as the ratio of cloudy *GMS-5* pixels to the total within each T2 footprint.

2) A NONLINEAR APPROACH FOR CLOUD DETECTION FROM THE 92- AND 150-GHZ CHANNELS.

A simple nonlinear cloud detection technique was developed based on the 92- and 150-GHz T2 window channels using a combination of the *GMS-5* derived cloud fraction data and model results. The two window channels were chosen due to their differential sensitivity to cloud. The 150-GHz channel is significantly more sensitive to cloud water and ice than the 92-GHz channel (Liu and Curry 1996). Figure 1a shows the observed variations in fractional cloudiness derived from the *GMS-5* visible channel data as a function of the 92- and 150-GHz Tb's. It is apparent from the figure that the cloud fraction increases for increasing 92-GHz Tb's and decreasing 150-GHz Tb's; however, this relationship is highly nonlinear. Precipitating clouds, especially those with a significant number of ice particles, produce the tail of very low 150-GHz Tb's associated with high 92-GHz Tb's evident in Fig. 1a. The sharp boundary defined by the clear-sky scenes can be approximated by a nonlinear exponential of the form:

$$\mathrm{Tb}_{150} = a[b - e^{(\mathrm{Tb}_{92} - c)/d}], \quad (1)$$

where a, b, c, and d are coefficients and Tb_{92} and Tb_{150} are the 92- and 150-GHz Tb's.

Simulated results of Tb's from the 92- and 150-GHz T2 channels for cloudy conditions are shown in Fig. 1b. Clear-sky transmittance values for air and water vapor were computed using the fast model of Eyre and Woolf (1988), and transmittance coefficients and single-scatter albedo values were computed from a very simple cloud model using coefficients given by Wu and Weinman (1984). The resulting Tb's were then computed using a discrete ordinate radiative transfer model developed by Stamnes et al. (1988). A number of simplifying assumptions were used in the model such as the exclusion of cloud ice and a constant surface emissivity of 0.7. As Fig. 1b shows, the relative variations in the 92- and

←

FIG. 3. A comparison of the T2 cloud index with corresponding cloud indicies from SSM/I and *GMS-5* for a swath between 60°N–60°S and 120°–180°E from 23 Jan 1998. The T2 cloud index is shown in (a) with a threshold value of 32 used for determining cloud/no-cloud effects on the 183-GHz channels, (b) with a threshold value of 12 for comparison with (c) the SSM/I-derived CLW and (d) the *GMS-5* visible albedo. The SSM/I-derived CLW and *GMS-5* visible albedo have been remapped into the T2 scan projection for ease of comparison. Values below the specified threshold values appear as the white regions. The three pixels at the end of each T2 scan are lost due to interference by the glare obstructor on DMSP *F14*.

150-GHz Tb's with increasing cloud amount are similar to the observed values, although the actual magnitude of the values differs significantly due to the simplifying assumptions made in the model. The simulated cloud amount is given in terms of a liquid water path as input to the model. The cloud fraction, which is derived from the cloud albedo, is highly correlated with the liquid water path (Stephens et al. 1984). Since the purpose of the simulated results was simply to show that the relative changes in Tb's with cloud amount is similar to the observed, no attempt was made to convert the observed cloud fraction to a liquid water path. Besides, the model does not include the effects of scattering by ice particles, which results in the tail seen in Fig. 1a.

The nonlinear exponential equation (1) was fit to the upper boundary defined by the clear-sky observations as shown in Fig. 1a using a standard nonlinear technique for minimizing a function of several variables. A simple equation relating a unitless cloud index to the observed Tb's was then developed by solving (1) for the variable *c*. Figure 1a shows a series of lines for different values of *c*, which roughly approximate the variations in cloud fraction. The resulting equation for computing the cloud index (I_{CLD}) from the 92- and 150-GHz T2 Tb's is as follows:

$$I_{\mathrm{CLD}} = \mathrm{Tb}_{92} - 170.57 + 23.94 \log\left[1.6725 - \frac{\mathrm{Tb}_{150}}{175.43}\right].$$

To determine the effect of clouds on the T2 UTWV channel, simulated Tb's computed from the PACS and CSP cruise radiosonde data were compared with observed values. The mean bias and standard deviation between the simulated and observed Tb's was computed using various cloud index threshold values. Statistics computed using only those matchups with cloud index values below the specified threshold are shown in Fig. 2. Using a relatively low cloud index threshold results in the lowest mean bias and standard deviation between the simulated and observed values; however, the majority of the observations are eliminated. Both the standard deviation and mean bias increase dramatically for cloud index threshold values above 32. While the effect is most evident in the 183 ± 7-GHz channel, a similar jump is apparent for the 183 ± 3- and 183 ± 1-GHz channels. For this reason, a cloud index threshold of 32 was chosen. Only T2 observations with cloud index values below 32 therefore were used in the clear-sky Tb time series.

A comparison of the T2 cloud index with cloud liquid water estimates from the DMSP SSM/I, based on the algorithm developed by Weng and Grody (1996) and *GMS-5* visible albedo, is shown in Fig. 3. The images are from 23 January 1998 from the DMSP *F14*, which is the only satellite with fully operational SSM/I and SSM/T2 sensors. All of the images have been registered into the T2 scan coordinates for ease of comparison. The black regions indicate land and/or missing data and, as can be seen by the shape of Australia in the lower part of the scan, have been warped by the registration into satellite image coordinates. The T2 cloud index is shown with two different thresholds applied. A value of 32 was used to indicate regions that are flagged as cloudy and a value of 12 was used to compare to the SSM/I liquid water estimates. This indicates that many of the low or nonprecipitating clouds pass through the T2 cloud detection test. Clouds with significant SSM/I-derived liquid water contents, however, correspond very well to the T2 cloud index. Statistics computed for a total of eight overpasses resulted in a correlation of 0.73 between the SSM/I CLW and T2 cloud index. The visible albedo values also correspond well with the T2 cloud index, except for the large system near the top of the scan, which is directly east of Japan (~35°–40°N). It is not clear why the storm system in the visible image appears farther east, but it may be due in part to the time differences between images. The correlation between the T2 cloud index and the *GMS-5* albedo was significantly lower at 0.45, although higher than the correlation between the SSM/I CLW and *GMS-5*, which was 0.38.

An analysis of variations in fractional cloudiness, as determined from *GMS-5* visible data, with scan position showed negligible differences across the scan, even though the view angle for the cross-track T2 scanner varies from nadir to 40.5° at the limb. Outside of the Tropics, however, the Tb's decrease along the nonlinear path described by (1). For this reason, the nonlinear approach was necessary in order to account for differences in both surface and cloud characteristics at different latitudes. Further investigation of scan angle effects as well as regional and seasonal variations remains to be done.

4. Intercomparison of modeled and observed Tbs

To understand the similarities and differences between the infrared HIRS channel 12 and the microwave T2 channel 2, a sensitivity analysis to changes in moisture and temperature was performed using radiative transfer model simulations from the TIGR-2 atmospheres. In addition, pentad averaged cloud-cleared Tb's from the two instruments were compared for an overlapping 1-yr period during 1995.

a. Sensitivity analysis

The normalized response functions for *GMS-5* channel 4 and HIRS channel 12 from *NOAA-11, -12,* and *-14* are plotted as a function of wavenumber in Fig. 4a. Both the *GMS-5* and HIRS-12 response functions reside between 1350 and 1550 cm^{-1} with the HIRS-12 instruments shifted toward slightly higher wavenumbers. Radiative transfer calculations were performed over this spectral region to illustrate where UTWV absorption is most significant. These calculations were made using

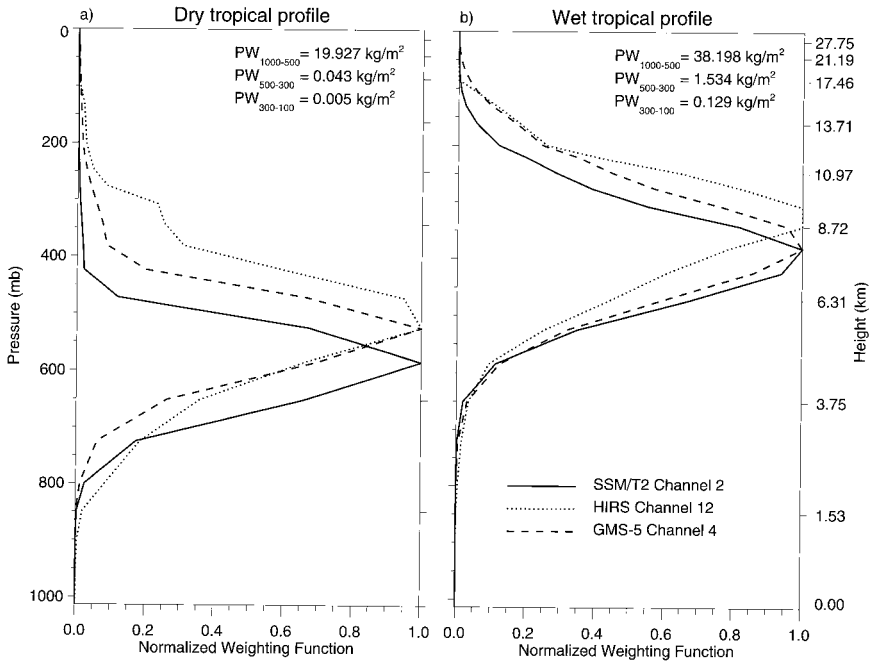

FIG. 5. Normalized weighting functions of the upper-tropospheric water vapor channels for the SSMT/2, HIRS, and *GMS-5* using a selected TIGR-2 (a) dry tropical atmospheric profile and (b) wet tropical atmospheric profile. The weighting function is defined as the change in transmittance with respect to the log of the pressure ($\partial\tau/\partial \ln P$).

MODTRAN 3 (Berk et al. 1989) and performed with the standard tropical atmosphere supplied by MODTRAN. Transmission values shown in Fig. 4b were calculated using atmospheric paths extending from 300 mb to the top of the atmosphere with a 10 cm^{-1} averaging window applied to the original 1 cm^{-1} resolution transmission values. A broad water vapor absorption region is shown from 1500 to 1550 cm^{-1} (6.7 μm). Carbon dioxide insignificantly affects the transmission for wavenumbers greater than 1375 cm^{-1}, and H_2O continuum effects are shown to be small for this upper-tropospheric path. The convolution of the filter response functions with the absorption line at 6.7 μm results in significantly lower Tb's from HIRS channel 12 than for the *GMS-5* instrument. This is due to the fact that the *GMS-5* response function is little weighted by the increased water vapor absorption for wavenumbers exceeding 1480 cm^{-1}, as shown in Fig. 4a.

A comparison of the normalized weighting functions between the IR instruments (*GMS-5* and *NOAA-12* HIRS) and the microwave T2 are shown in Fig. 5. Weighting functions from *NOAA-11* and *-14* HIRS were not included since they were found to be almost identical to the profiles computed for *NOAA-12*. Radiative transfer calculations of the transmission profile for all three instruments were performed on two vastly different tropical profiles. The profile shown in Fig. 5a typifies the persistent subsidence regions in the subtropics with warm temperatures but relatively little moisture, while the profile shown in Fig. 5b is characteristic of the intertropical convergence zone with very warm temperatures and substantial moisture at all levels. For the moist profile, shown in Fig. 5b, the HIRS instrument peaks at around 325 mb, while the *GMS-5* and T2 instruments peak at around 375 mb. A comparison of a number of different profiles indicates that the weighting functions of *GMS-5* and T2 generally peak lower in the troposphere. The weighting function of *GMS-5* is lower than that for the HIRS channel 12 since its response function peaks to the wing of the 6.7-μm absorption band. Figure 5a shows that for the dry profile, the weighting function peaks at 600 mb for all but the T2 instrument, which peaks at 650 mb. The IR instruments also show more sensitivity to increases in moisture at levels above 400 mb.

Figure 6a shows a comparison between simulated T2 channel 2 Tb's and the two IR channel simulations using the tropical TIGR-2 profiles. Results show that both IR simulations have a positive slope of about 0.75 indicating that the T2 Tb's have wider dynamic range for this set of observations. The lower Tb's from the HIRS channel 12 instrument are indicative of its increased sensitivity to high-level moisture due to the proximity of the response function to the 6.7-μm water vapor line. This is a direct result of the *GMS-5* weighting function lying just below the 6.7-μm water vapor absorption region, as was indicated earlier. Figure 6b shows a similar plot of the relationship between the observed T2 channel 2 and HIRS channel 12 Tb's averaged for 1995. Insufficient data was available from *GMS-5* for it to be in-

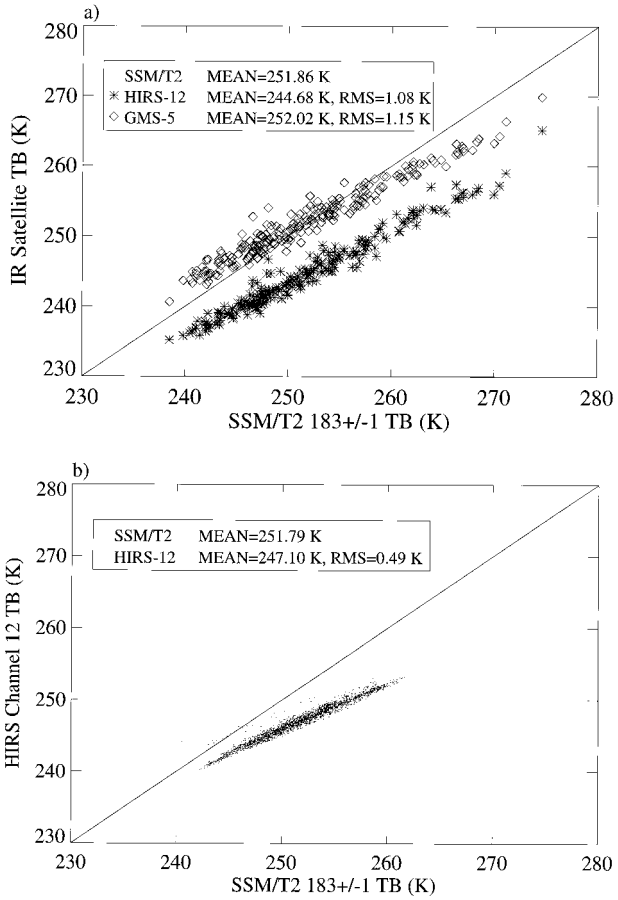

FIG. 6. Scatter diagram of (a) simulated T2 channel 2 Tb's plotted vs simulated *GMS-5* channel 4 and *NOAA-12* HIRS channel 12 Tb's using 227 TIGR-2 tropical profiles and (b) observed annual Tb's for 1995 from T2 channel 2 plotted vs HIRS channel 12.

cluded in the comparison. The observed relationship is very similar to the simulated results; however, the rms difference is slightly lower and the range of values is somewhat less, which is most likely due to the long-term averaging. The mean Tb's are also a couple of degrees warmer for both instruments with a similar offset between the two means.

A sensitivity analysis of the modeled T2 and HIRS Tb's to changes in temperature and moisture was carried out for the tropical TIGR-2 profiles. The sensitivity of the HIRS simulations was found to be analogous to the *GMS-5*; therefore, only the HIRS simulations are presented here. This involved two sets of analyses: 1) comparing simulated Tb's as a function of three vertical layer mean relative humidity (RH) values: 100–300, 300–500, and 500–1000 mb; and 2) perturbing the temperature and moisture profiles in these three layers a ''small'' amount in order to identify the differences in the sensitivity of HIRS and T2 instruments. Because the T2 and HIRS water vapor channels are sensitive to both water vapor and temperature, the Tb's are more highly correlated to RH than water vapor mixing ratio or overburden. All RH perturbations were constrained between 0% and 100%. It should be noted that the RH values were computed with respect to liquid water as is the convention with radiosonde data. As a result, cold upper-tropospheric temperatures can reduce the RH maximum from 100% to as little as 70% due to saturation with respect to ice. The first two layers were chosen to quantify the sensitivity each instrument has at different levels of the upper troposphere.

The comparison of simulated Tb's between T2 and HIRS channel 12 is shown in Fig. 7 for three different layers. Logrithmic scaling is used on the RH axis. Figure 7a shows a weak relationship between the Tb's and the log of the RH within the 100–300-mb layer for both the T2 and HIRS instruments. The 300–500-mb layer results shown in Fig. 7b gives the tightest fit to this logarithmic relationship. This agrees with the findings of Soden and Bretherton (1994) and Stephens et al. (1996), who used this relationship to develop upper-tropospheric humidity retrieval methods. The 500–1000-mb layer results shown in Fig. 7c indicate significant scatter and no relationship between RH and the simulated Tb's for either instrument.

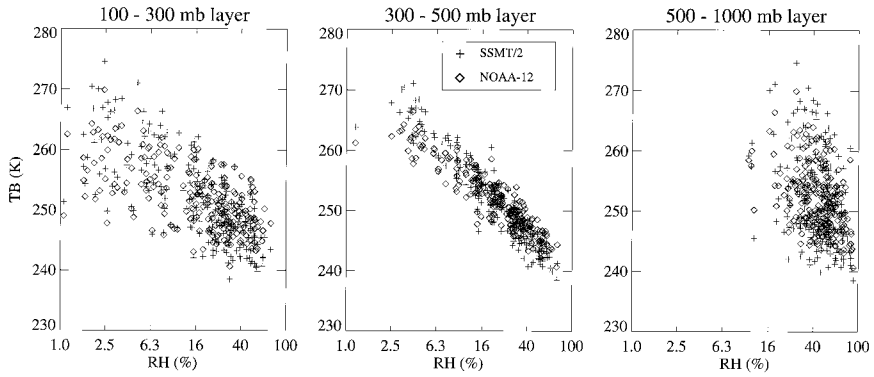

FIG. 7. The RH vs Tb for both T2 channel 2 and HIRS channel 12 from *NOAA-12* simulated using the TIGR-2 atmospheres. Logarithmic scaling is used on the RH axis. Plots are shown for three different atmospheric layers including (a) 100–300, (b) 300–500, and (c) 500–1000 mb.

TABLE 1. Modeled Tb perturbations using tropical TIGR-2 profiles and perturbating the RH profile by ±10%. Slope, mean, and rms difference indicate the scatterplot summary statistics between T2 channel 2 and HIRS channel 12 (H12) Tb's. ΔTb columns show the Tb changes when perturbing the RH to the indicated layers.

	T2/H12 slope	T2/H12 mean difference	T2/H12 rms difference	H12 ΔTb	T2 ΔTb
TIGR +10% RH (100–1000 mb)	1.33	5.99	1.35	−3.71	−4.90
TIGR +10% RH (100–300 mb)	1.30	6.23	1.41	−1.57	−2.52
TIGR +10% RH (300–500 mb)	1.23	6.05	1.29	−1.98	−3.12
TIGR +10% RH (500–1000 mb)	1.23	6.87	1.27	−0.44	−0.76
TIGR NO CHANGE	1.28	7.18	1.42	0.00	0.00
TIGR −10% RH (100–1000 mb)	1.01	7.46	2.51	6.41	6.69
TIGR −10% RH (100–300 mb)	1.23	7.79	1.56	1.54	2.14
TIGR −10% RH (300–500 mb)	1.24	8.20	1.65	2.66	3.68
TIGR −10% RH (500–1000 mb)	1.27	7.45	1.62	0.98	1.25

The sensitivity of the T2 and HIRS Tb's to moisture and temperature perturbations is described here as difference in Tb from the perturbed case and the nonperturbed case [ΔTb = Tb(perturbed) − Tb(nonperturbed)]. A sensitivity analysis where the RH field was modified by 10% (holding temperature constant) and an analysis where temperature was modified by 2 K (holding specific humidity constant) was performed. These values were chosen arbitrarily in order to illustrate the sensitivity differences between T2 and HIRS and are not intended to explain observed differences in the T2 and HIRS Tbs. Because the interest for climate studies is on systematic differences, random errors due to instrument noise were considered to be negligible when averaged over a large number of individual samples and are therefore ignored. Tables 1 and 2 summarize the results of the perturbation analysis. As shown in these tables, the results are essentially symmetric for positive and negative perturbations in temperature but not for changes in RH. The T2 has the strongest sensitivity to moisture perturbations, and both instruments have a similar sensitivity to temperature perturbations. For a 10% increase in RH in the highest levels (100–300 mb), the T2 Tb's drop by 4.90 K, while the HIRS Tb's drop by only 3.71 K. The change for a 10% decrease in RH, however, is even larger with a Tb increase of 6.69 K for the T2 and 6.41 K for HIRS.

The sensitivity of HIRS Tb's to the water vapor continuum effects was examined using MODTRAN-3, which models the continuum using the method described by Clough et al. (1992). It was found that the continuum contribution to the Tb was slightly dependent on latitude with a 1.61 K increase in temperature for the tropical profiles and a 1.15 K increase in temperature for the polar profiles. These results agree well with the findings of Stephens et al. (1996).

b. Comparison of observed SSM/T2 and HIRS-12 Tb's

Cloud-cleared Tb's were computed for both the T2 channel 2 (from DMSP *F12*) and HIRS channel 12 (from *NOAA-11, -12,* and *-14*) for a 1-yr period during 1995. The Tb's were composited over 2.5° × 2.5° bins and 5 days. Figure 8 shows the mean and standard deviation of the T2 channel 2 Tb's as well as the standard deviation of the HIRS channel 12 Tb's.

The mean cloud-cleared Tb map shown in Fig. 8a indicates the maximum values occurring in the cloud-free region of the eastern Pacific just south of the equator. Similar maxima occur in the southern tropical regions just west of Australia and Africa, with minima occurring in the convective regions of the western Pacific warm pool and the ITCZ regions. The regions of maximum Tb's correspond to extremely dry air in the upper troposphere associated with strong subsidence,

TABLE 2. Modeled Tb perturbations using tropical TIGF-2 profiles and perturbating the temperature profile by ±2 K. Slope, mean, and rms difference indicate the scatterplot summary statistics between T2 channel 2 and HIRS channel 12 (H12) Tb's. ΔTb columns show the Tb changes when perturbing the temperature to the indicated layers.

	T2/H12 slope	T2/H12 mean difference	T2/H12 rms difference	H12 ΔTb	T2 ΔTb
TIGR +2 K (100–1000 mb)	1.28	7.34	1.43	1.94	2.10
TIGR +2 K (100–300 mb)	1.27	7.27	1.41	0.45	0.53
TIGR +2 K (300–500 mb)	1.27	7.41	1.39	1.08	1.30
TIGR +2 K (500–1000 mb)	1.30	7.42	1.47	0.43	0.66
TIGR NO CHANGE	1.28	7.18	1.42	0.00	0.00
TIGR −2 K (100–1000 mb)	1.28	7.02	1.43	−1.94	−2.10
TIGR −2 K (100–300 mb)	1.30	7.08	1.44	−0.43	−0.53
TIGR −2 K (300–500 mb)	1.30	6.93	1.46	−1.06	−1.31
TIGR −2 K (500–1000 mb)	1.26	6.93	1.39	−0.42	−0.67

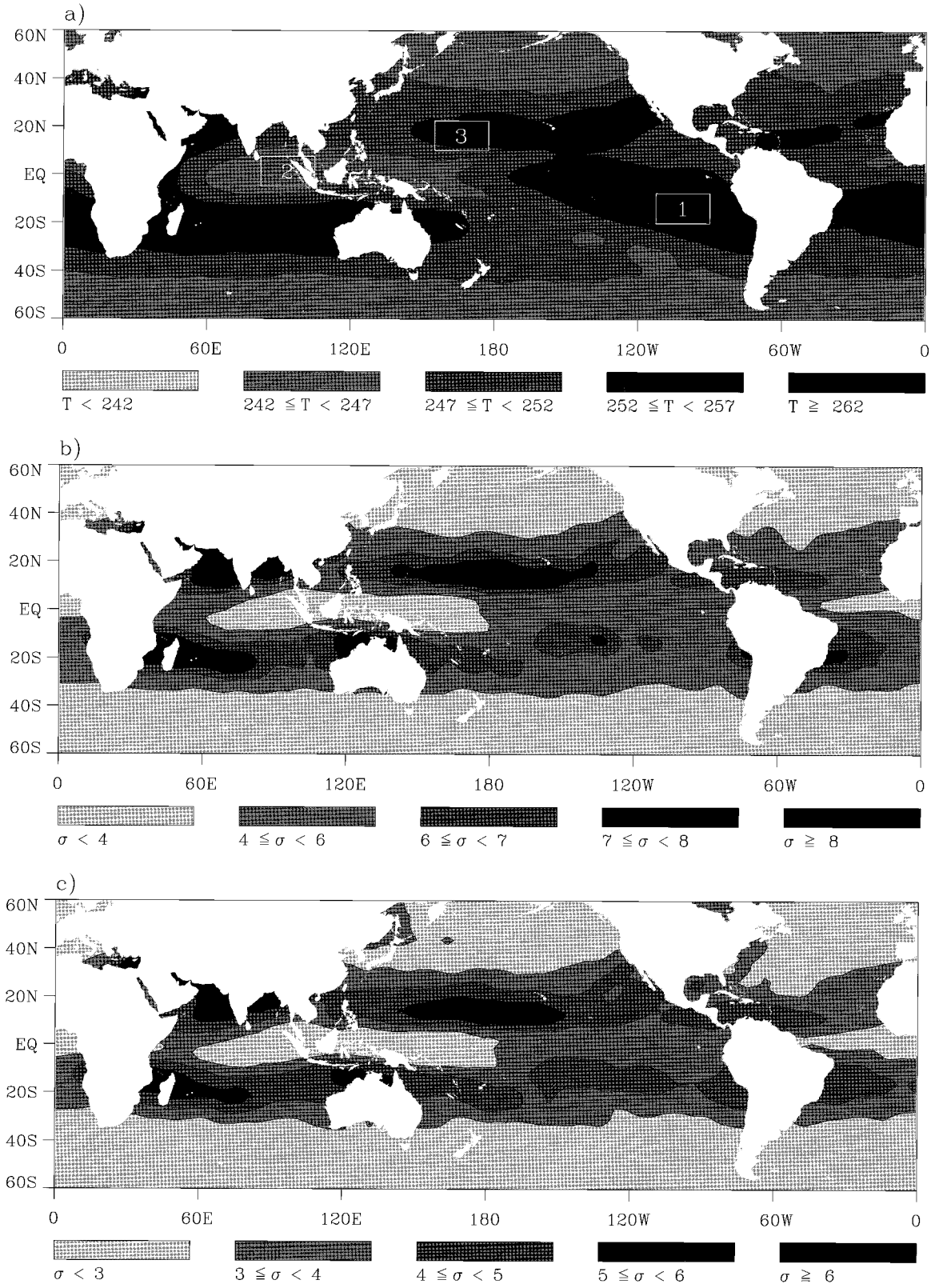

FIG. 8. Maps of (a) T2 channel 2 mean Tb's, (b) T2 channel 2 std dev's, and (c) HIRS channel 12 std dev's. These statistics were computed from time series of clear-sky Tb's averaged over 2.5° × 2.5° bins and 5 days during 1995.

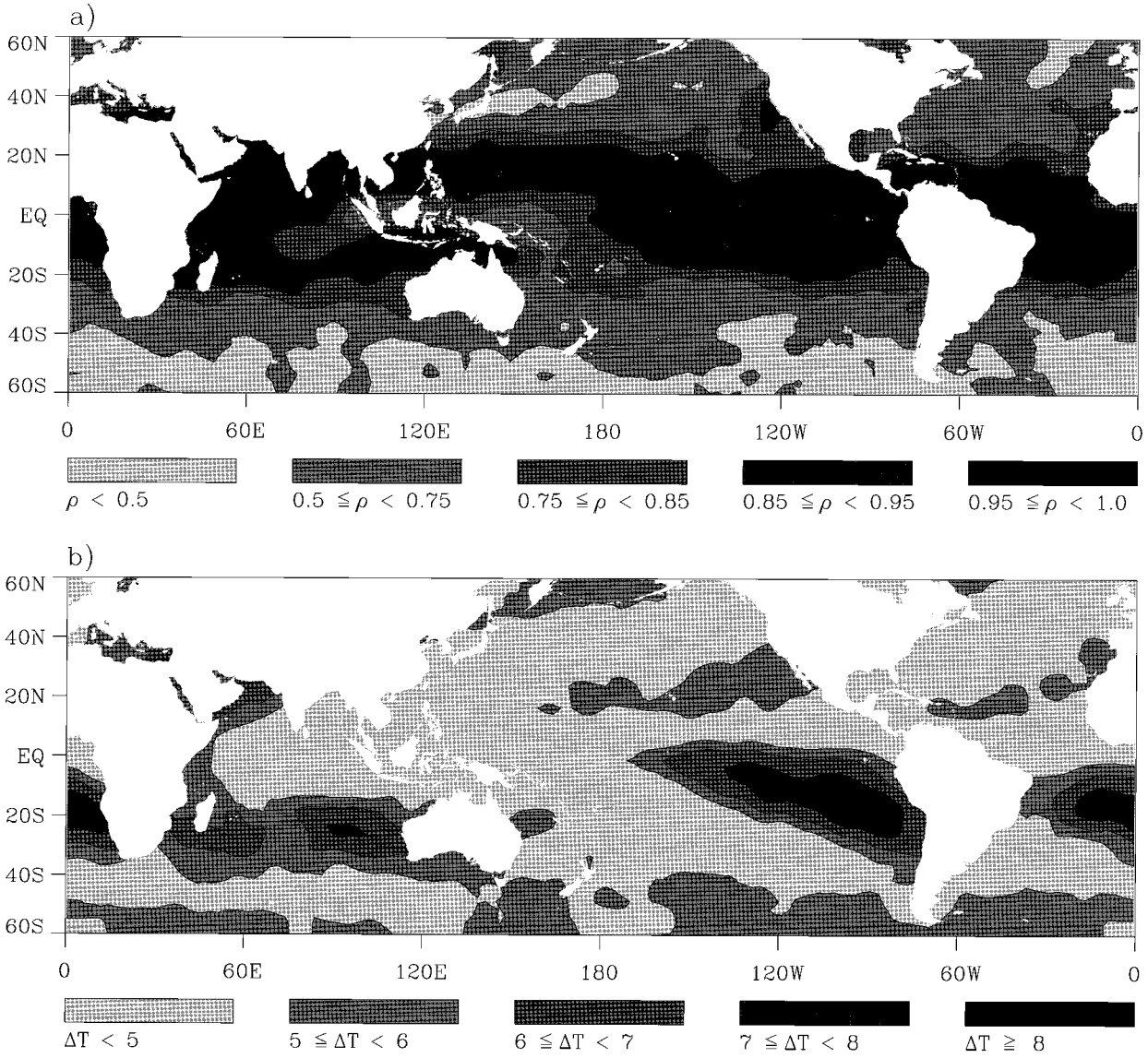

FIG. 9. Spatial maps of the (a) correlations and (b) differences (T2 − HIRS) between T2 channel 2 and HIRS channel 12 clear-sky Tb's from the same pentad time series used in Fig. 8.

while the minimums tend to correspond to the convective zones. The standard deviation maps for the T2 and HIRS, shown in Figs. 8b and 8c, respectively, indicate the largest variability in the northern Tropics over regions with a strong (large amplitude) annual cycle in UTWV. The lowest variability occurs over the convective zones. The range of values shown in Fig. 8b is larger than that of the HIRS because of the increased sensitivity of the T2 to changes in UTWV, as discussed in section 4a.

A correlation map of the pentad time series is shown in Fig. 9a and a map of the mean Tb differences (T2 − HIRS) is shown in Fig. 9b. Figure 9a indicates that the highest correlations occur along the northern tropical belt, corresponding to regions with a strong annual cycle in UTWV, and in the cloud-free regions of the tropical east Pacific. The largest differences, shown in Fig. 9b, occur in the ocean desert region off the western coast of South America where the mean Tb's are at their peak (Fig. 8a). The differences are largest in the dry zones because the IR sensor is more sensitive to moisture at the highest levels, as shown in Fig. 5.

The correlations drop off dramatically outside of the Tropics for a number of reasons. First, regions of persistent cloudiness result in fewer clear-sky sounding observations by the infrared HIRS instrument. Stratus and cirrus clouds obscure the moisture signal in the IR, although, as shown in Fig. 3, the T2 instrument is insensitive to these types of clouds. Second, the relative contribution of temperature and moisture to changes in Tb

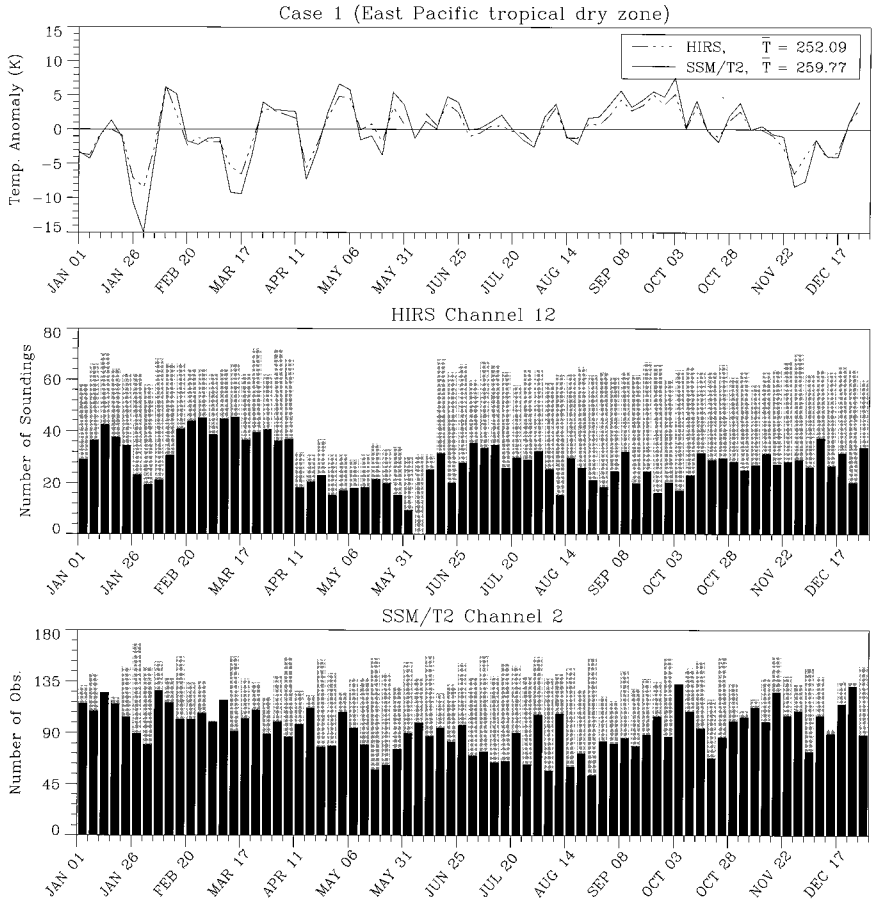

FIG. 10. A comparison of the Tb time series from T2 channel 2 and HIRS channel 12 during 1995. The values have been averaged over 45 2.5° × 2.5° bins for the region from 7.5° to 20.0°S and 90° to 112.5°W within the eastern Pacific dry zone. (a) T2 channel 2 and HIRS channel 12 Tb time series with the annual means removed. (b) HIRS average number of estimated soundings (light gray) and clear-sky number of soundings (black) for a 2.5° bin. (c) The T2 average number of observations (light gray) and clear-sky number of observations (black) for a 2.5° bin.

increases at higher latitudes for HIRS channel 12 data. In the Tropics, not only are the temperature and moisture profiles highly correlated but the moisture signal dominates the resulting Tb's. Unlike the T2, in the midlatitudes the lower moisture contents result in an increased sensitivity of the HIRS-12 to changes in temperature. As a result, the infrared HIRS and microwave T2 agree very well in the relatively cloud-free regions of the Tropics, but that agreement falls off quickly at higher latitudes. Lower correlations over the convective zones are due to a decrease in clear-sky observations, especially by the HIRS instrument, and less variability in the clear-sky Tb time series.

To better understand the differences in the Tb's from HIRS channel 12 and T2 channel 2, the time series were spatially averaged for three regions with very different characteristics. The three regions selected are shown in the mean T2 Tb map in Fig. 8a. Case 1 is over the region of maximum temperatures in the cloud-free region of the eastern Pacific, case 2 is over the region of maximum convection in the western Pacific warm pool, and case 3 is over the northern subtropics where the annual cycle is particularly strong.

The Tb time series for case 1 are shown with the mean values removed in Fig. 10. Bar charts indicating the number of clear-sky and the total number of observations for both HIRS and T2 are also shown in this figure. Similar plots for cases 2 and 3 are shown in Figs. 11 and 12, respectively, and a summary of the statistics for these three cases is given in Table 3. The time series shown in Fig. 10 indicate significant variability over monthly timescales, with the maximum deviations occurring around the end of January, during which time both time series show a drop in the number of clear-sky observations. Note that the sudden decrease in the total number of observations from HIRS during April and May is due to the loss of *NOAA-11*. In general, both time series show a significant percentage of clear-

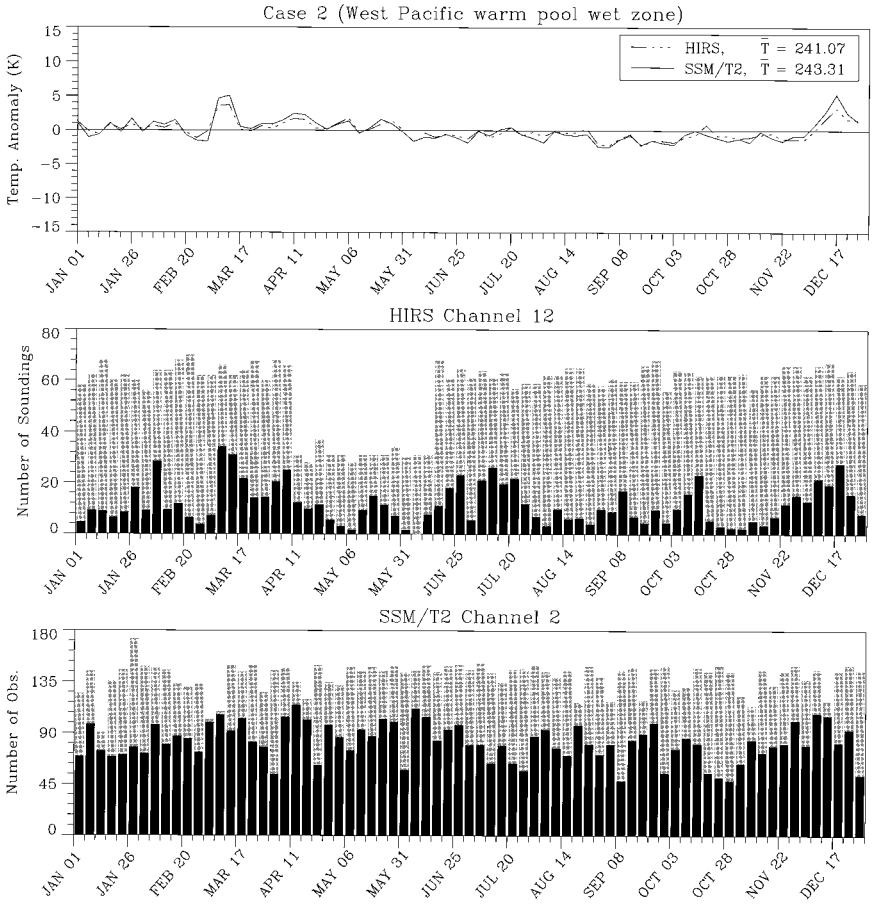

FIG. 11. The same as Fig. 10 but for the region from 5.0°S to 7.5°N and 82.5° to 105.0°E covering a total of 45 2.5° × 2.5° bins over the western Pacific warm pool.

sky observations for this region resulting in a correlation of 0.97. The lower sensitivity of the T2 instrument to nonprecipitating clouds, however, results in a significantly higher percentage of clear-sky observations. Although HIRS data were available from two satellites over most of the year versus a single satellite for the T2, the total number of observations for T2 is significantly larger. This is due primarily to lower spatial resolution of the HIRS soundings (~90 km versus ~50 km for T2).

The time series for case 2 over the western Pacific warm pool shown in Fig. 11 indicates much less variability in the clear-sky Tb's. This is consistent with the perturbation analysis summarized in Table 1, which shows significantly larger changes in Tb's for moisture perturbations in dry conditions than wet ones. As a result, the correlation between the two time series is slightly lower at 0.94. As expected for a convective region, the number of clear-sky observations is significantly lower for both instruments but markedly so for the HIRS soundings. From Table 3, 60% of the T2 observations are identified as clear versus 21% for HIRS. This clearly shows the advantage of the microwave T2 instrument in monitoring UTWV over cloudy regions.

The results for case 3, shown in Fig. 11, indicate a strong annual cycle and a correlation of 0.98. As Table 3 indicates, the standard deviation is very large for both instruments due to the strong annual cycle. It is apparent, therefore, that the seasonal variability is accurately captured by both instruments and that the differences in the cloud detection schemes have minimal impact on the resulting variability observed between these two time series.

5. Conclusions

To compare Tb observations sensitive to UTWV between the infrared HIRS channel 12 and the microwave T2 channel 2, a technique was developed for detecting T2 Tb's influenced by either liquid water and ice clouds. A nonlinear cloud index developed from the T2 92- and 150-GHz window channels shows good agreement with cloud liquid water retrievals derived from SSM/I. Comparisons of simulated and observed Tb's with varying

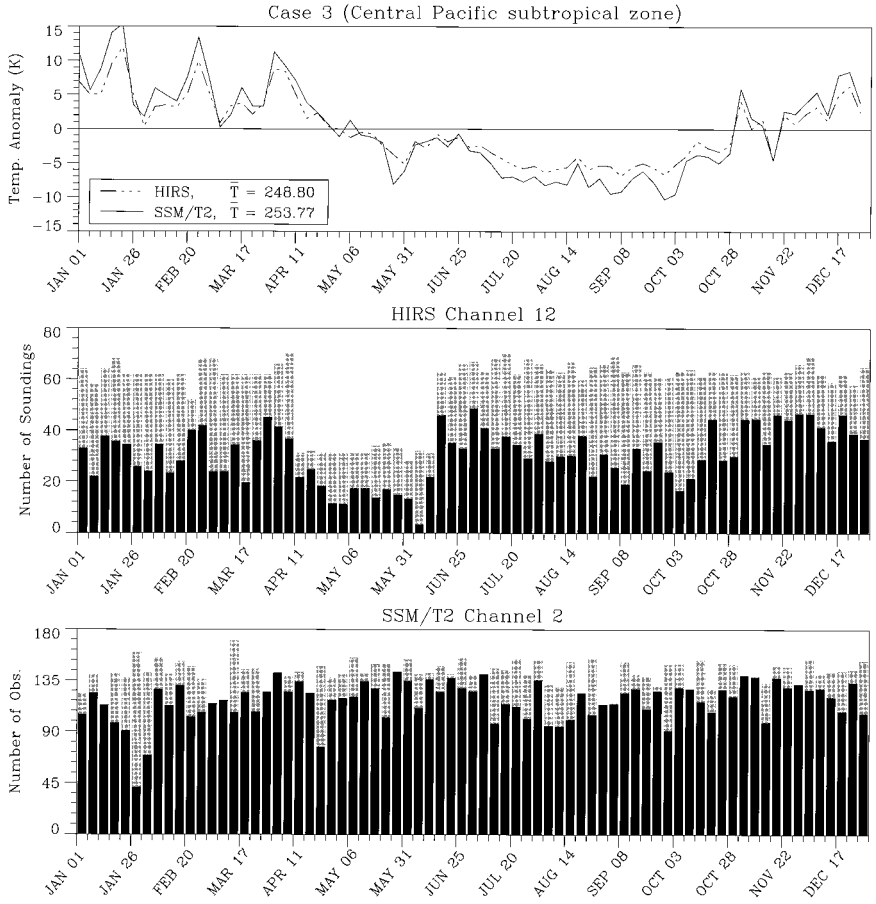

FIG. 12. The same as Fig. 10 but for the region from 10.0° to 22.5°N and 155.0° to 177.5°E covering a total of 45 2.5° × 2.5° bins over the central Pacific subtropics.

cloud index threshold values show an insensitivity of the T2 mid- and upper-tropospheric water vapor channels to most nonprecipitating clouds. As a result, the microwave sensor has a distinct advantage over the IR sensors in monitoring UTWV over cloudy regions such as the western Pacific warm pool, which minimizes any climatological dry bias in the microwave UTWV Tb time series.

An analysis of simulated Tb's using the TIGR-2 radiosonde profiles shows that the microwave T2 instrument is more sensitive to moisture perturbations than either the HIRS and *GMS-5* IR sensors by about 25%. HIRS channel 12, however, peaks highest in the troposphere and is most sensitive to moisture above 400 mb. The *GMS-5* UTWV channel peaks slightly lower in the troposphere since its response function peaks to the wing of the 6.7-μm absorption band. The T2 UTWV channel peaks lower than either of the IR sensors but has a narrower weighting function, which results in its increased sensitivity to moisture perturbations. A strong

TABLE 3. Statistics between the T2 channel 2 and HIRS channel 12 pentad Tb's during 1995 for the three averaged time series cases shown in Figs. 10, 11, and 12. The statistics shown include the case number, the number of bins averaged together, the number of observations in the time series, the correlation coefficient, the number of effective degrees of freedom, and the mean difference. Also shown are the mean, standard deviation, and percentage of clear-sky pixels for both the HIRS and the T2 time series. The units for the mean and standard deviations are in Kelvins, while the number of observations are the average for a 2.5° × 2.5° bin within the selected region.

						HIRS			T2		
Case	Bins	Obs	Corr. coef.	Eff. DOF	Mean diff	Mean	Std	Clear	Mean	Std	Clear
1	45	72	0.97	40	7.68	252.09	3.13	51.8%	259.77	4.39	69.3%
2	45	72	0.94	35	2.24	241.07	1.23	21.4%	243.31	1.63	59.7%
3	45	73	0.98	14	4.96	248.80	4.66	56.3%	253.77	6.47	85.4%

relationship between Tb and the log of the RH is evident for both the HIRS channel 12 and T2 channel 2 within the layer from 300 to 500 mb.

A comparison of clear-sky observed Tb's averaged over 2.5° × 2.5° bins and 5 days during 1995 shows good agreement between the infrared and microwave observations of UTWV in the Tropics. The HIRS and T2 channels are most highly correlated in relatively cloud-free regions like the east Pacific just south of the equator and in regions with a strong annual cycle in UTWV, such as is the case over the North Pacific subtropical zone. The correlations between the microwave T2 and infrared HIRS are significantly lower, however, in the midlatitudes and over regions with signficant cloud cover. This is due primarily to differences between climate regimes, which include changes in both the temperature and moisture profiles and thus the level and depth of the atmospheric layer being observed. In addition, sensitivity to clouds and the cloud detection algorithms used and sampling differences are especially significant over convective regions and areas of persistant cloudiness. The relative insensitivity of the T2 channels to stratus or other nonprecipitating clouds gives the microwave instrument a significant advantage in observing UTWV over these regions. The availability of HIRS data back to 1979, however, provides a valuable long-term record of UTWV observations for climate studies.

The upcoming launch of AMSU on NOAA-K will provide higher-resolution observations at or very near the frequencies used by the current HIRS and T2 channels. This will greatly simplify the task of intercomparing the microwave and infrared upper-tropospheric water vapor channels. The availability of HIRS data from 1979 and T2 data from 1993, however, will remain important for longer-term climate studies.

Acknowledgments. The authors wish to thank Merritt Deeter for his assistance with the radiative transfer simulations of the PACS and CSP radiosonde datasets and Tony McNally at NESDIS for his help in answering questions about the HIRS sounding data used in this study.

REFERENCES

Bates, J. J., X. Wu, and D. L. Jackson, 1996: Interannual variability of upper-troposphere water vapor band brightness temperature. *J. Climate,* **9,** 427–438.

Berk, A., L. S. Bernstein, and D. C. Robertson, 1989: MODTRAN: A moderate resolution model for LOWTRAN 7. Spectral Sciences, Burlington, MA, 38 pp. [Available from Spectral Sciences, Inc., 99 South Bedford St., 7, Burlington, MA 01803.]

Clough, S. A., M. J. Iacono, and J.-L. Moncet, 1992: Line-by-line calculations of atmospheric fluxes and cooling rates: Application to water vapor. *J. Geophys. Res.,* **97,** 15 761–15 785.

Eyre, J. R., 1990: The information content of data from satellite sounding systems: A simulation study. *Quart. J. Roy. Meteor. Soc.,* **116,** 401–434.

——, and H. M. Woolf, 1988: Transmittance of atmospheric gases in the microwave region: A fast model. *Appl. Opt.,* **27,** 3244–3249.

Kidwell, K. B., 1995: NOAA Polar Orbiter data (*TIROS-N, NOAA-6, NOAA-7,* and *NOAA-8*) users guide. NOAA, Washington, D.C., 381 pp.

Lindzen, R. S., 1990: Some coolness concerning global warming. *Bull. Amer. Meteor. Soc.,* **71,** 288–299.

Liu, G., and J. A. Curry, 1996: Large-scale cloud features during January 1993 in the North Atlantic Ocean as determined from SSM/I and SSM/T2 observations. *J. Geophys. Res.,* **101,** 7019–7032.

McMillin, L. M., and C. Dean, 1982: Evaluation of a new operational technique for producing clear radiance. *J. Appl. Meteor.,* **21,** 1005–1014.

——, and A. Nappi, 1986: Some modifications to the NESDIS operational clear column radiance procedure. *Third Int. TOVS Study Conf.,* Madison, WI, Cooperative Institute for Meteorological Satellite Studies, University of Wisconsin, 160–172.

McNally, A. P., and M. Vesperini, 1996: Variational analysis of humidity information from TOVS radiances. *Quart. J. Roy. Meteor. Soc.,* **122,** 1521–1544.

Moine, P., A. Chedin, and N. A. Scott, 1987: Automatic classification of air mass type from satellite vertical sounding data. Application to *NOAA-7* observations. *Ocean–Air Interactions,* **1,** 95–108.

Rosenkranz, P. W., M. J. Komichak, and D. H. Staelin, 1982: A method for estimation of atmospheric water vapor profiles by microwave radiometry. *J. Appl. Meteor.,* **21,** 1364–1370.

Soden, B. J., and F. P. Bretherton, 1994: Evaluation of water vapor distribution in general circulation models using satellite observations. *J. Geophys. Res.,* **99,** 1187–1210.

——, and J. R. Lanzante, 1996: An assessment of satellite and radiosonde climatologies of upper-tropospheric water vapor. *J. Climate,* **9,** 1235–1250.

Spencer, R. W., and J. R. Christy, 1993: Precision lower stratospheric temperature monitoring with the MSU: Technique, validation, and results 1979–1991. *J. Climate,* **6,** 1194–1204.

Stamnes, K., S. C. Tsay, W. Wiscombe, and K. Jayaweera, 1988: Numerically stable algorithm for discrete-ordinate-method radiative transfer in multiple scattering and emitting layered media. *Appl. Opt.,* **27,** 2502–2509.

Stephens, G. L., S. Ackerman, and E. A. Smith, 1984: A shortwave parameterization revised to improve cloud absorption. *J. Atmos. Sci.,* **41,** 687–690.

——, D. L. Jackson, and I. Wittmeyer, 1996: Global observations of upper-tropospheric water vapor derived from TOVS radiance data. *J. Climate,* **9,** 305–326.

Velden, C. S., C. M. Hayden, S. J. Nieman, W. P. Menzel, S. Wanzong, and J. S. Goerss, 1997: Upper tropospheric winds derived from geostationary satellite water vapor observations. *Bull. Amer. Meteor. Soc.,* **78,** 173–195.

Wang, J. R., J. Zhan, and P. Racette, 1997: Storm-associated microwave radiometric signatures in the frequency range of 90–220 GHz. *J. Atmos. Oceanic Technol.,* **14,** 13–31.

Weng, F., and N. C. Grody, 1994: Retrieval of cloud liquid water using the special sensor microwave/imager. *J. Geophys. Res.,* **99,** 25 535–25 551.

Wilheit, T. T., 1990: An algorithm for retrieving water vapor profiles in clear and cloudy atmospheres from 183-GHz radiometric measurements: Simulation studies. *J. Appl. Meteor.,* **29,** 508–515.

Wu, R., and J. A. Weinman, 1984: Microwave radiances from precipitating clouds containing aspherical ice, combined phase, and liquid hydrometeors. *J. Geophys. Res.,* **89,** 7170–7178.